

# Photoactivation experiment on $^{197}\text{Au}$ and its implications for the dipole strength in heavy nuclei

C. Nair,<sup>1</sup> M. Erhard,<sup>1</sup> A. R. Junghans,<sup>1</sup> D. Bemmerer,<sup>1</sup> R. Beyer,<sup>1</sup> E. Grosse,<sup>1,2</sup> J. Klug,<sup>1,\*</sup> K. Kosev,<sup>1</sup> G. Rusev,<sup>1,†</sup> K. D. Schilling,<sup>1</sup> R. Schwengner,<sup>1</sup> and A. Wagner<sup>1</sup>

<sup>1</sup>*Institut für Strahlenphysik, Forschungszentrum Dresden-Rossendorf, D-01314 Dresden, Germany*

<sup>2</sup>*Institut für Kern- und Teilchenphysik, Technische Universität Dresden, D-01062 Dresden, Germany*

(Dated: November 28, 2008)

The  $^{197}\text{Au}(\gamma, n)$  reaction is used as an activation standard for photodisintegration studies on astrophysically relevant nuclei. At the bremsstrahlung facility of the superconducting electron accelerator ELBE of FZ Dresden-Rossendorf, photoactivation measurements on  $^{197}\text{Au}$  have been performed with bremsstrahlung endpoint energies from 8.0 to 15.5 MeV. The measured activation yield is compared with previous experiments as well as calculations using Hauser-Feshbach statistical models. It is shown that the experimental data are best described by a two-lorentzian parametrization with taking the axial deformation of  $^{197}\text{Au}$  into account. The experimental  $^{197}\text{Au}(\gamma, n)$  reaction yield measured at ELBE via the photoactivation method is found to be consistent with previous experimental data using photon scattering or neutron detection methods.

PACS numbers: 25.20.-x, 25.20.Dc, 26.30.-k

## I. INTRODUCTION

Photonuclear processes are among the first nuclear reactions ever studied in the laboratory [1]. They have provided important information about the giant dipole resonance (GDR) [2] and play a vital role in our understanding of the cosmic nucleosynthesis pointed out by Burbidge et al. [3]. In high temperature cosmic scenarios like exploding supernovae, the photon flux is intense enough to cause the photodisintegration of previously formed heavy nuclides. The photonuclear cross sections are of importance for the understanding of neutron capture in hot and neutron rich stellar environments, where nuclei are likely to be excited from their ground states and may simultaneously undergo capture. The usual laboratory study of radiative neutron capture does not yield direct information on such processes, but their inverse, photon induced neutron emission to excited states may reveal respective information via the detailed balance principle [4].

More generally, the combined information from photodisintegration and photon scattering allows to derive the photon strength function (PSF) below and above the separation energies. The PSF is an essential ingredient for the modeling of astrophysical reaction rates for network calculations of the cosmic nucleosynthesis. The other component of such investigations is the Hauser-Feshbach statistical model (HFM). Accurate experimental studies of the excitation functions of photon induced processes allow sensitive tests of the parameters entering the model calculations, - e.g., optical-model potentials, level densities

and transmission coefficients.

From photoneutron studies concentrating on the GDR region, the accuracy needed for a detailed prediction of the yields of heavy nuclei produced by neutron capture via s- and r-processes cannot be reached [5]. For the neutron-deficient p-nuclei, there is practically no experimental data existing in the astrophysically relevant energy region [6]. In view of the emerging novel observations of isotopic yields in stellar plasma and in gathered cosmic material, high accuracy network calculations are of increasing interest.

The photoneutron cross section of  $^{197}\text{Au}$  has been measured by various methods. It has been shown that the cross sections in the isovector GDR region as measured at different laboratories may differ beyond their statistical and systematic uncertainties [2]. Recently, the photoneutron cross section of  $^{197}\text{Au}$  has been measured with laser-induced Compton backscattered (LC) photons at the TERAS storage ring at AIST Tsukuba, Japan [7]. Photoactivation of Au has also been investigated recently with bremsstrahlung at an extremely stable clinical accelerator [8].

The  $^{197}\text{Au}(\gamma, n)$  reaction is used as an activation standard for photodisintegration studies on astrophysically relevant nuclei. In this paper we present a study of the  $^{197}\text{Au}(\gamma, n)$  reaction for the whole region from the neutron threshold  $S_n$  to beyond the top of the GDR with an accuracy of nearly 10%. The bremsstrahlung endpoint energies for the measurements range from 8.0 to 15.5 MeV. Special care was taken at each accelerator setting to measure the bremsstrahlung endpoint energy without relying on the magnetic beam transport elements. The photon flux was determined by an independent observation of photon scattering from  $^{11}\text{B}$  exposed to the same photons as the Au samples. The residual nucleus  $^{196}\text{Au}$  produced from the  $^{197}\text{Au}(\gamma, n)$  reaction was studied by  $\gamma$ -ray spectroscopy.

Secs. II and III describe the experimental procedure

\*Present address: Ringhals Nuclear Power Plant, SE-43022 Väröbacka, Sweden

†Present address: Department of Physics, Duke University, Triangle Universities Nuclear Laboratory, Durham, NC 27708, USA.

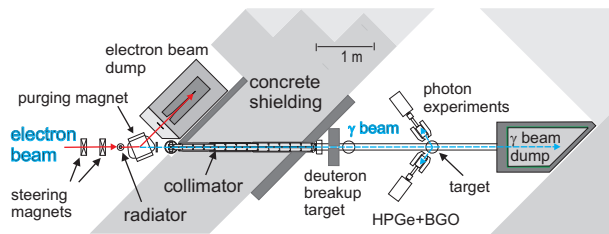


FIG. 1: (Color online) The bremsstrahlung facility at ELBE. The Au targets were irradiated together with  $^{11}\text{B}$  samples at the target site. The photons scattered from  $^{11}\text{B}$  samples were measured using four 100% HPGe detectors with BGO escape-suppression shields, two of which were mounted vertically (not shown). The endpoint energy of the bremsstrahlung was determined from the proton spectrum of the deuteron breakup reaction.

and the data analysis. In Sec. IV A, the experimental activation yield is compared to the yield calculated using cross sections from previous experiments on  $^{197}\text{Au}(\gamma, n)$ .

In Sec. IV B, the experimental yield is compared with Hauser-Feshbach model calculations. It is shown that the predictions of these models deviate from the measured activation yield.

A phenomenological parametrization of the photon strength function is proposed which describes the experimental data and extrapolates it well to the threshold region. Sec. IV C of this paper is devoted to the description of this parametrization and to its comparison with data from photoneutron and photon-scattering studies as well as the comparison with other descriptions of the photon strength function.

## II. EXPERIMENTAL SETUP

The experiments were performed at the superconducting electron accelerator ELBE (Electron Linear accelerator of high Brilliance and low Emittance) of the Forschungszentrum Dresden-Rossendorf. ELBE can produce intense bremsstrahlung beams with endpoint energies from 6 to 18 MeV. With these beam parameters both photon scattering and photodisintegration reactions have been measured [9, 10, 11, 12, 13].

The bremsstrahlung facility is shown in Fig. 1. The electron beam is focused onto a niobium radiator with thicknesses varying between  $1.7 \text{ mg/cm}^2$  and  $10 \text{ mg/cm}^2$  (corresponding to  $1.6 \cdot 10^{-4}$  and  $1 \cdot 10^{-3}$  radiation lengths) which creates typical "thin target" bremsstrahlung. After passing the radiator, the electrons are deflected by a dipole magnet and dumped to a graphite cylinder mounted on insulating rods surrounded by a water cooled vacuum vessel (electron beam dump, see figure). A collimator placed 1 m behind the radiator is used to form a beam with defined diameter out of the spatial distribution of photons. The collimator is made from high-purity aluminum and is fixed within the 1.6 m thick wall

of heavy concrete between the accelerator hall and the experimental cave. An aluminum cylinder of 10 cm diameter and 10 cm length placed in a vacuum chamber in front of the entrance of the collimator acts as a hardener which absorbs mainly low energy photons and thus 'hardens' the photon spectrum.

At the target site, the bremsstrahlung beam is collimated onto the  $^{197}\text{Au}$  targets sandwiched with a  $^{11}\text{B}$  sample. The photon flux is determined experimentally by means of the known integrated cross sections of the states in  $^{11}\text{B}$  depopulating via  $\gamma$  rays. Photons scattered from  $^{11}\text{B}$  are measured with four high-purity germanium (HPGe) detectors of 100% relative efficiency which are surrounded by escape-suppression shields consisting of bismuth-germanate (BGO) scintillation detectors. The experimental procedure has been described in detail elsewhere [14, 15].

The  $^{197}\text{Au}$  targets used were thin discs with a typical mass of about 200 mg, thickness 0.02 mm, and diameter 20 mm. The number of activated nuclei produced during the activation was determined offline by measuring the decay of daughter nuclei in a low-level counting setup by HPGe detectors with relative efficiencies of 90% or 60%.

The endpoint energy of the bremsstrahlung distribution is determined by measuring protons from the photodisintegration of the deuteron (see Fig. 1, deuteron breakup target) with silicon detectors. From the maximum energy of the emitted protons, the maximum energy of the incident photons can be deduced. This is described in detail in Sec. III C. During the experiment, energy drifts of the electron linac have been kept to below 1% using non-destructive beam-diagnostics of the transverse beam dispersion and an active beam-stabilization control loop.

## III. DATA ANALYSIS

The data deduction and analysis methods will be described in detail in the following sections. The discussion is split into three parts:

- (A) Decays observable following the  $^{197}\text{Au}(\gamma, n)$  reaction and determination of the photoactivation yield;
- (B) Experimental determination of the photon flux at the scattering site; and
- (C) Bremsstrahlung endpoint energy determination using the deuteron breakup reaction.

### A. $^{196}\text{Au}$ decay

The  $^{197}\text{Au}(\gamma, n)$  reaction produces the unstable nucleus  $^{196}\text{Au}$  which decays either to  $^{196}\text{Pt}$  by electron capture or positron emission ( $\text{EC}+\beta^+$ ) or to  $^{196}\text{Hg}$  by beta-decay ( $\beta^-$ ). A typical decay spectrum of a  $^{197}\text{Au}$  sample irradiated with a bremsstrahlung endpoint energy of

TABLE I: Decay properties of the  $^{196}\text{Au}$  nucleus.

Nuclide <sup>a</sup>	$E_\gamma$ (keV) <sup>b</sup>	$p^c$
$^{196}\text{Pt}$	333.03(5)	0.229(10)
$^{196}\text{Pt}$	355.73(5)	0.87(3)
$^{196}\text{Hg}$	426.10(8)	0.066(3)

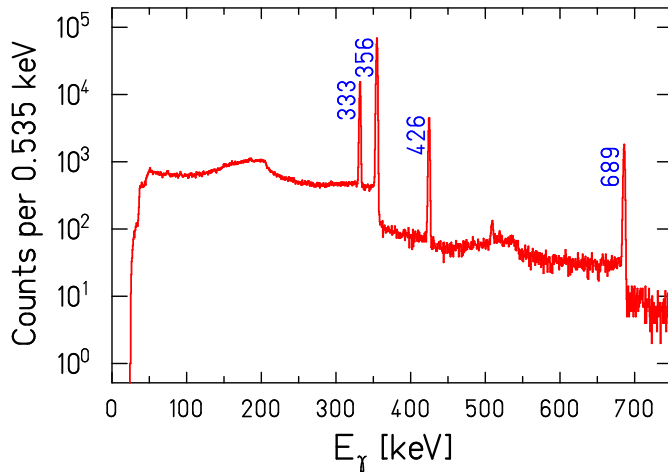
<sup>a</sup>Daughter nuclide from  $^{196}\text{Au}$  decay<sup>b</sup>Energy of the transition with absolute uncertainty given in parentheses.<sup>c</sup>Photon emission probability per decay with absolute uncertainty given in parentheses.

FIG. 2: (Color online) Spectrum of an irradiated  $^{197}\text{Au}$  target. The target was placed on the top of a HPGe detector with 90% relative efficiency. The peaks originating from the  $^{196}\text{Au}$  decay are marked. The  $\gamma$ -line at 689 keV is the sum of the  $\gamma$ -transitions with energies 333 and 356 keV. A 1.5 mm thick Cd absorber was used to suppress coincidence summing and low energy X-rays.

14.5 MeV for 17 hours is given in Fig. 2. The prominent peaks in the decay of  $^{196}\text{Au}$  used for analysis are marked in Fig. 2 and are given in Table I. The decay properties given in the table are adopted from Ref. [16].

The absolute photopeak efficiency of the counting setup has been determined with several calibration sources from PTB and Amersham (systematic uncertainty in activity 0.6-1.5%) in the energy range from 0.12 to 1.9 MeV [1]. The absolute efficiency was simulated for a realistic geometry using the Monte Carlo code GEANT3 [17] and was fitted to the measured data. Coincidence summing effects depend strongly on the decay scheme. They were determined very precisely for

the corresponding counting geometry. The distance between the surface of the endcap and detector crystal was cross-checked by X-ray radiography. The number of  $\gamma$ -rays counted in the peaks at 333 and 356 keV have been corrected for 'summing-out' events using the method described in Ref. [18]. For the transition at 333 keV, the coincidence summing correction amounts to 24% and for 356 keV it is 6%, both with a relative uncertainty of 5%.

In a photoactivation experiment, the number of radioactive nuclei  $N_{\text{act}}(E_0)$  produced is proportional to the integral of the absolute photon fluence  $\Phi_\gamma(E, E_0)$  times the photodisintegration cross section  $\sigma_{\gamma,n}(E)$  integrated from the reaction threshold energy  $E_{\text{thr}}$  up to the end-point energy  $E_0$  of the bremsstrahlung spectrum.

$$N_{\text{act}}(E_0) = N_{\text{tar}} \cdot \int_{E_{\text{thr}}}^{E_0} \sigma_{\gamma,n}(E) \cdot \Phi_\gamma(E, E_0) dE \quad (1)$$

The number of radioactive nuclei  $N_{\text{act}}(E_0)$  is determined experimentally by measuring the activity of the irradiated sample using:

$$N_{\text{act}}(E_0) = \frac{N_\gamma(E_\gamma, E_0) \cdot \kappa_{\text{corr}}}{\varepsilon(E_\gamma) \cdot p(E_\gamma)} \quad (2)$$

$N_\gamma(E_\gamma, E_0)$ ,  $\varepsilon(E_\gamma)$ ,  $p(E_\gamma)$  denote the dead-time and pile-up corrected full-energy peak counts of the observed transition, the absolute efficiency of the detector at the energy  $E_\gamma$  and the emission probability of the photon with energy  $E_\gamma$ , respectively.

The factor  $\kappa_{\text{corr}}$  in Eq. (2) is given by

$$\kappa_{\text{corr}} = \frac{\exp\left(\frac{t_{\text{loss}}}{\tau}\right)}{1 - \exp\left(\frac{-t_{\text{meas}}}{\tau}\right)} \cdot \frac{\frac{t_{\text{irr}}}{\tau}}{1 - \exp\left(\frac{-t_{\text{irr}}}{\tau}\right)} \quad (3)$$

This expression determines the number of radioactive nuclei from their decays measured during the time  $t_{\text{meas}}$ . It also takes into account decay losses during irradiation ( $t_{\text{irr}}$ ) and in between the end of the irradiation and the beginning of the measurement ( $t_{\text{loss}}$ ). The mean life time of the radioactive nucleus produced during the photoactivation is denoted by  $\tau$ . The decay time constants of  $^{196}\text{Au}$  and  $^{198}\text{Au}$  have been confirmed in a precision measurement using targets produced in the scope of the present experiment [19].

The activation yield is denoted by  $Y_{\text{act}}$  and is expressed as the ratio of the number of activated nuclei to the number of target atoms in the sample. For the  $^{197}\text{Au}(\gamma, n)$  reaction,

$$Y_{\text{act}} = \frac{N_{\text{act}}(^{196}\text{Au})}{N_{\text{tar}}(^{197}\text{Au})} \quad (4)$$

Using Eq. (1), the activation yield can be calculated from  $\sigma_{\gamma,n}(E)$  data with the known bremsstrahlung spectrum. In this way measured activation yields can be compared with the experimental or theoretical cross section data.

[1] PTB: Physikalisch-Technische Bundesanstalt, Fachbereich 6.1, Bundesallee 100, Braunschweig, Germany;  
Amersham: ISOTRAK AEA Technology QSA, Gieselweg 1, Braunschweig, Germany.

## B. The photon flux

In the present study, the photon flux was determined from the elastic photon scattering from a  $^{11}\text{B}$  sample sandwiched with the Au activation target. Four HPGe-detectors (two at  $90^\circ$  and two at  $127^\circ$ ) were used for this measurement (see Ref. [14] for details). The photon fluence is determined experimentally using the formula:

$$\Phi_\gamma(E_\gamma) = \frac{N_\gamma(E_\gamma)}{\varepsilon(E_\gamma) \cdot N_{\text{tar}} \cdot I_s \cdot W(\theta)} \quad (5)$$

$N_\gamma(E_\gamma)$ ,  $\varepsilon(E_\gamma)$ ,  $N_{\text{tar}}$  represents the dead-time and pile-up corrected full-energy peak counts of the resonant transition, the absolute efficiency of the detector at the energy  $E_\gamma$ , and the number of target atoms in the  $^{11}\text{B}$  sample.  $W(\theta)$  is the angular correlation between the incoming and scattered photon and  $I_s$  denotes the integrated scattering cross section.

The decay properties of calibration transitions were adopted from the online library of Evaluated Nuclear Structure Data Files (ENSDF) which refers to the revised Ajzenberg-Selove compilation (see Table 11.4, Ref. [20]). The absolute photopeak efficiency has been determined with calibration sources for energies up to 1.9 MeV. For extrapolating the efficiency to higher energies, a GEANT3 simulation under realistic geometry was used (see Fig.4, Ref. [13]). The simulations were normalized to the measured efficiency at energies below 1.9 MeV.

In a typical case, the  $^{11}\text{B}$  target used was of metallic boron powder with an enrichment of 99.5%, mass areal density of  $1.43 \text{ g cm}^{-2}$ , and an effective density of  $1.6 \text{ g cm}^{-3}$ . Energy dependent nuclear self absorption corrections were applied using the formalism given in Ref. [21]. For example, for the transition at 7.288 MeV, the nuclear self absorption correction amounts to about 7.5% when using a target with the specifications given above.

The bremsstrahlung spectrum is well approximated by the theoretical bremsstrahlung distribution for a thin niobium target. Different approaches are compared for the niobium radiator for an incident electron endpoint energy of 11.5 MeV as shown in Fig. 3. They agree well with recent quantum mechanical calculations by Haug [24, 25] which use the atomic shielding effects given in Ref. [26].

At the low-energy side of the spectrum the different theoretical approaches are not distinguishable from each other and agree within 1 percent. Near endpoint, the theoretical models differ by about 20% (see inset, Fig. 3). The theoretical description of the high-energy end of the bremsstrahlung distribution has a systematic effect on the calculation of the activation yield from a given photon-neutron cross section (see section IV A). For an endpoint energy of 9 MeV or higher, the  $^{197}\text{Au}(\gamma, n)$  activation yield calculated with the cross section from Haug would be 5% lower than that calculated with the cross section from Seltzer and Berger. Below 9 MeV this effect increases up to 30%.

The experimental photon fluence determined from the  $^{11}\text{B}(\gamma, \gamma')$  reaction for the  $\gamma$ -transitions at 2.125,

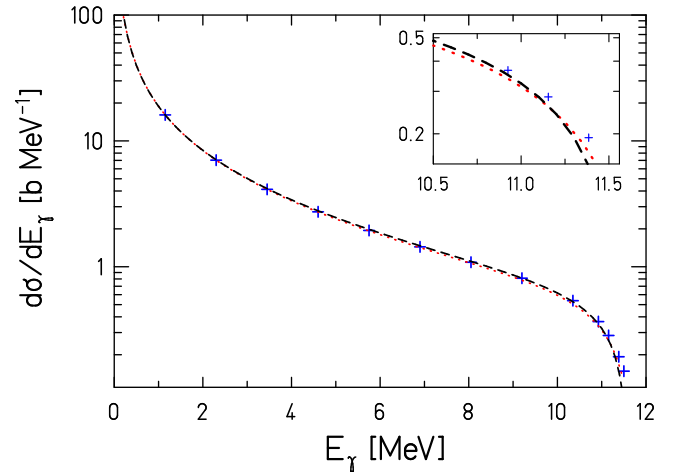


FIG. 3: (Color online) Comparison of theoretical bremsstrahlung cross sections for the Nb radiator for an incident electron endpoint energy of 11.5 MeV. Dashed and dotted lines correspond to the bremsstrahlung distributions by Schiff [22] and Haug [24] whereas values created from the Seltzer and Berger [23] tables are shown as symbols (+).

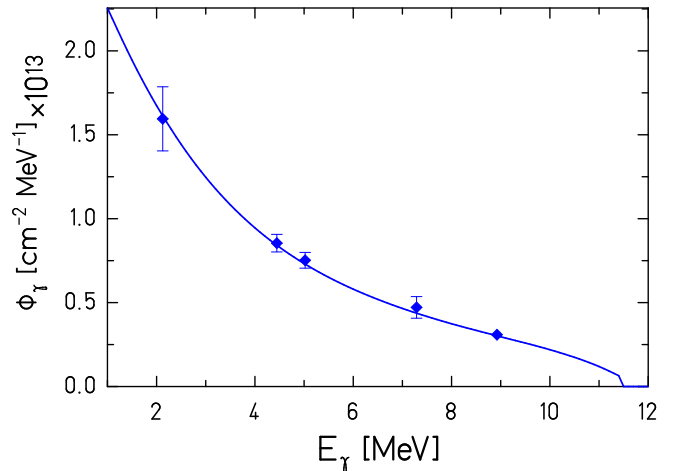


FIG. 4: (Color online) Absolute photon fluence measured from the scattered photons in  $^{11}\text{B}$  is compared with the Seltzer and Berger bremsstrahlung spectra with hardener corrections. The fluence measured with different transitions in  $^{11}\text{B}$  agree to the simulated curve to within 6%.

4.446, 5.022, 7.288, and 8.924 MeV are shown in Fig. 4. The bremsstrahlung spectrum was simulated using MCNP [27] to take into account the effects of the aluminum hardener situated behind the niobium radiator. In MCNP, the bremsstrahlung cross sections from Seltzer and Berger are used. The simulated bremsstrahlung spectrum has been normalized to the measured absolute photon fluence at the transition energies of  $^{11}\text{B}$ . The systematic deviations between the simulated curve and the experimental points are about 6%.

In the fluence determination procedure discussed above, the statistical contribution to the uncertainties from the gamma-counting is quite small and is of the order of 0.5-2%. The systematic uncertainty in the extrapolation of efficiency is estimated to be about 5% in the energy range of the observed transitions in  $^{11}\text{B}$ .

### C. Determination of bremsstrahlung endpoint energy

For the experiments described here, it is necessary to measure the endpoint energy of the bremsstrahlung spectra precisely. An on-line measurement of the beam energy is attained using the dispersion inside a dipole magnet with a magnetic field integral  $\int B dl$  known to about 1% only [28]. Therefore, we employed a different method for the beam energy determination which is based on the spectroscopy of protons in the photodisintegration of the deuteron - the  $^2\text{H}(\gamma, p)n$  reaction. From the pure two-body kinematics, the energy of the incident photon can be deduced directly from the measured energy of the emitted proton.

The protons from the photodisintegration of the deuteron are detected by a setup of four silicon detectors (Ion-Implanted-Silicon Charged-Particle Detectors, type ORTEC ULTRA [2]) placed at a distance of 115 mm from the beam axis and at azimuthal angles of  $0^\circ$ ,  $90^\circ$ ,  $180^\circ$  and  $270^\circ$  with respect to the photon beam. The detectors have a thickness of  $500\text{ }\mu\text{m}$  and a sensitive area of  $600\text{ mm}^2$ . A  $4\text{ mg/cm}^2$  thick polyethylene film, in which hydrogen is substituted by deuterium ( $\text{CD}_2$ ) [3] is used as a target. The  $\text{CD}_2$  target is positioned parallel to the incident beam such that its surface is observed by all four detectors under  $45^\circ$ . A typical spectrum is shown in Fig. 5. The low-energy part of the spectrum below 2.5 MeV is not useful as it is dominated by beam induced background.

In order to determine the endpoint energy, a simulated spectrum is fitted to the measured proton spectrum. The simulation takes into account the deuteron breakup kinematics, geometry of the detector setup, energy loss of the protons inside the  $\text{CD}_2$  film as well as the energy spread of the electron beam. The fit to the measured spectra is shown in Fig. 6. The statistical error from the fit amounts to 2-8 keV for the range of energies described here. The systematic deviation of the experimental spectra to the simulated one is 40 keV. This is inherent to all experiments but significant only for endpoint energies close above the neutron-emission threshold of  $^{197}\text{Au}(\gamma, n)$  reaction.

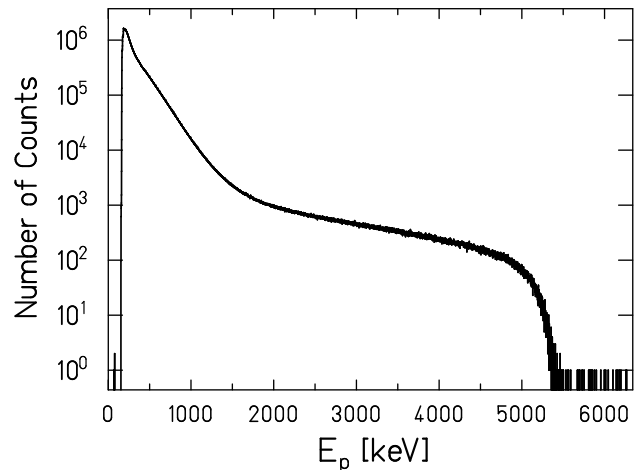


FIG. 5: Proton spectrum from the photodisintegration of deuterons, recorded with Si detectors of  $500\text{ }\mu\text{m}$  thickness during an irradiation with incident electron energy 13.2 MeV.

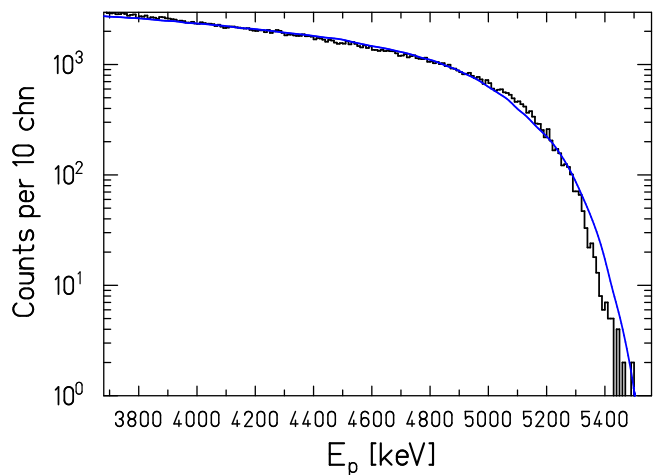


FIG. 6: (Color online) The simulated proton spectrum (line) is fitted to the measured spectrum (histogram) from Fig. 5.

## IV. RESULTS AND DISCUSSION

Photoactivation experiments with bremsstrahlung have the limitation that the data need to be unfolded to obtain a cross section [29]. This requires precise knowledge of the bremsstrahlung spectrum especially close to the endpoint, and data with very high counting statistics on a fine grid of endpoint energies. In this work, the measured photoactivation yield is presented and compared to calculated yield curves.

For the  $^{197}\text{Au}(\gamma, n)$  reaction, the photoactivation yield is determined as described by Eq. (4). The activation yield is normalized to the photon fluence for the corresponding measurement as discussed in Sec. III B. The endpoint energies were determined from the photodisintegration of the deuteron as explained in Sect. III C. The

[2] ORTEC, 801 South Illinois Avenue, Oak Ridge, TN 37830, USA.

[3] Courtesy : D. K. Geiger, SUNY Geneseo, NY 14454, USA.



experimental activation yield normalized to the photon fluence is compared with previous experimental data as well as model calculations.

### A. Activation Yield : Comparison with previous experiments

In this section, the activation yield from the ELBE experiments is compared to calculated yields using cross sections measured in previous experiments. A comparison of the  $^{197}\text{Au}(\gamma, n)$  cross sections from previous experiments [30, 31, 32, 33] is given in Fig. 7. At the Lawrence Livermore National Laboratory (LLNL), the photoneutron cross section of the nucleus  $^{197}\text{Au}$  has been measured with quasi-monoenergetic photons from the positron annihilation technique. There are two sets of published data - first by Fultz et al. [30] and later by Berman et al. [31]. The same technique has been used by Veyssiere et al. [32] at Saclay (France) for studying photoneutron reactions on  $^{197}\text{Au}$ . The results from Livermore and Saclay are not in agreement, revealing the differences in the neutron multiplicity determination procedure used in both laboratories.

Berman et al. have remeasured photoneutron cross sections with quasi-monoenergetic photons at LLNL, with special emphasis on determining the absolute cross section at energies across the peak of the GDR. Based on this experiment, Berman et al. resolves the differences by recommending a 7% scaling on the Veyssiere data and ignoring the Fultz data (see Table VI, Ref. [31]). We adopt this recommendation for comparing the ELBE data with the previously reported values.

At the Laser-Compton scattering facility at the TERAS storage ring at AIST Tsukuba, quasi-monoenergetic photons were used to study photoneutrons from  $^{197}\text{Au}(\gamma, n)$  up to 12.4 MeV. These data agree very well with the data measured with the positron annihilation technique but as a photon difference method was used they have a rather large experimental uncertainty.

The photoneutron cross section of  $^{197}\text{Au}$  for energies close above the  $(\gamma, n)$  threshold has been deduced by Vogt et al. [33] using photoactivation with bremsstrahlung at the S-DALINAC (Darmstadt). The cross sections are in agreement with Veyssiere et al., but exist only for endpoint energies between 8.0 MeV and 10.0 MeV.

The total nuclear photoabsorption cross section of  $^{197}\text{Au}$  was measured at the synchrotron facility of the Institute of Nuclear Research (Moscow) by Gurevich et al. [34]. Even though the data agree with the measurements by Veyssiere et al., they exhibit significant scatter (Fig. 2, Ref. [34]). The tabulated errors are quite big and therefore were not included for comparison with the ELBE data reported here. The photoneutron yield for  $^{197}\text{Au}$  was measured by Sorokin et al. [35], at the Betatron (Moscow State University) and the cross sections were deduced by the Penfold-Leiss [36] method. This experiment was done with an energy resolution of 0.5

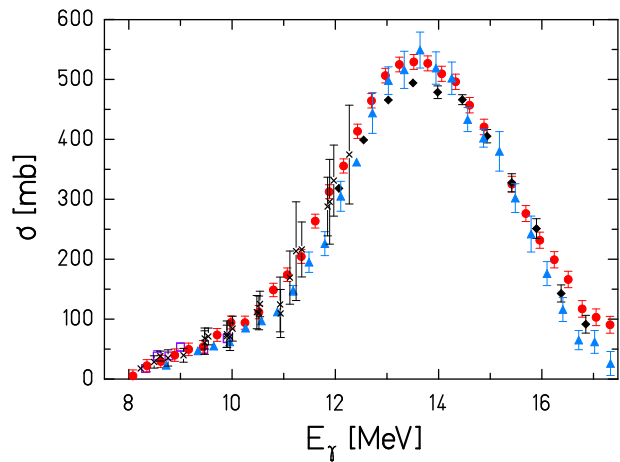


FIG. 7: (Color online) Photoneutron cross sections for  $^{197}\text{Au}(\gamma, n)$  from previous experiments. The symbols denote data from the respective experiments : triangles - Fultz et al. [30], diamonds - Berman et al. [31], circles - Veyssiere et al. [32]. Some  $^{197}\text{Au}(\gamma, n)$  cross section data below 10 MeV have been derived from bremsstrahlung activation by Vogt et al. (open squares) [33]. Also shown are cross sections determined from Laser-Compton scattering by Hara et al. ( $\times$ ) [7].

MeV for the range of energies considered here. The results from Sorokin et al. are not included in the present discussion because the uncertainties resulting from the unfolding process are very large and the data differ significantly from the previous experimental data.

In Fig. 8, the experimental activation yield from ELBE is compared to the yield calculated using the cross sections measured previously. The activation yield is normalized to the photon fluence measured from the scattered photons in  $^{11}\text{B}$  (see Sect. III B). The experimental yield from ELBE is in agreement with the yield calculated using the cross sections from Vogt et al. for the close-threshold endpoint-energies up to 10 MeV. The activation yield calculated using cross sections from Veyssiere et al. is in agreement with the ELBE yield for the whole range of energies. Close to the neutron emission threshold, the reaction yield strongly depends on the endpoint energy  $E_0$  of the bremsstrahlung beam. In this case, small uncertainties in  $E_0$  result in large uncertainties of the activation yield.

The uncertainties in the experimental points shown in Fig. 8 are mainly from the determination of photon fluence as discussed in Sec. III B. The statistical uncertainties are very small and in the order of about 0.5-2%. The major systematic uncertainties arise from the extrapolation of measured photopeak efficiencies to the higher energies in  $^{11}\text{B}$  transitions (5%) and in the systematic deviation of measured photon fluence from the simulated curve (6%). The systematic errors have been added quadratically and amount to about 7.8% but are not shown in Fig. 8.

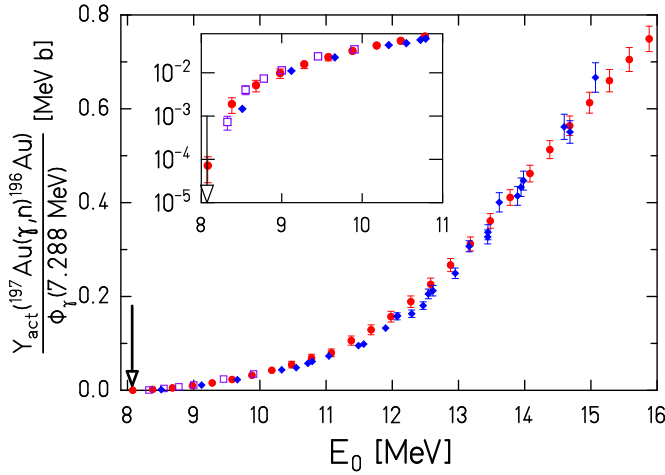


FIG. 8: (Color online) Activation yield for the  $^{197}\text{Au}(\gamma, n)$  reaction normalized to the photon fluence is compared to the yield calculated using cross sections measured in previous experiments. The present data are denoted by diamonds with an arrow pointing to the neutron emission threshold. Reaction yield calculated using the cross sections given by Veyssiere et al. [32] (circles) and Vogt et al. [33] (open squares) are in good agreement with the yield measured at ELBE.

### B. Activation Yield : Comparison with model calculations

Fig. 9 compares the experimental activation yield to the simulated yield calculated using cross sections predicted by Hauser-Feshbach models [37, 38]. Simulations using the TALYS [37] and NON-SMOKER [38] codes describe the experimental data only to a factor of 2. Both calculations were performed using cross sections derived from standard input parameters. The default option of TALYS for the GDR parameters originates from the Beijing GDR compilation, as present in the RIPL database [39].

In the case of  $(\gamma, n)$  reactions, one crucial ingredient for the model calculation is the photon strength function. As the  $(\gamma, n)$  channel in  $^{197}\text{Au}$  is the dominant decay channel for the energy range above threshold, the photon strength distribution directly determines the calculated  $(\gamma, n)$  cross section and the reaction yield. In the model calculations care is also taken for the fact that the  $(\gamma, p)$  channel is open above 5.8 MeV. Due to the large  $Z$ , the  $p$ -emission is strongly suppressed by the Coulomb interaction. With default inputs, the TALYS calculation yields a  $(\gamma, p)$  cross section which is about four orders of magnitude smaller than the  $(\gamma, n)$  cross section.

The activation yields calculated using TALYS with different optical model potentials, like Koning-Delaroché and Jeukenne-Lejeune-Mahaux (JLM), are very similar demonstrating that the  $^{197}\text{Au}(\gamma, n)$  reaction yield is not sensitive to the choice of optical model parameters. The sensitivity to the photon strength function is larger. We

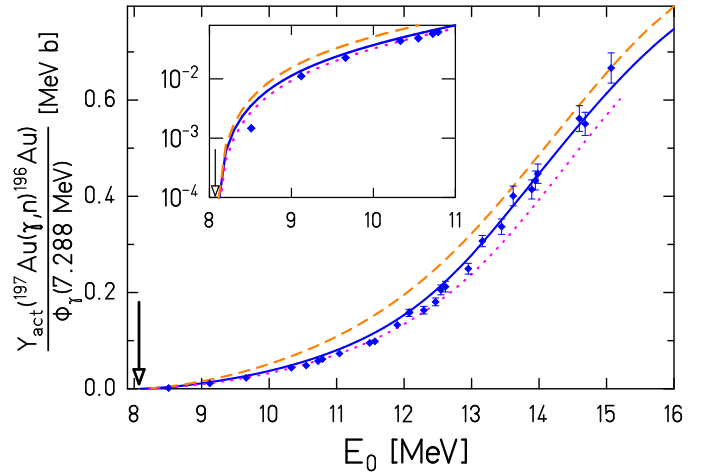


FIG. 9: (Color online) Experimental activation yield normalized to the photon fluence for the  $^{197}\text{Au}(\gamma, n)$  reaction compared to theoretical model calculations. The experimental data are denoted by diamonds with a downward arrow denoting the neutron emission threshold. The dashed and dotted lines denote yield calculations using cross sections from the TALYS [37] and NON-SMOKER [38] codes respectively. The solid line represents a TALYS calculation with modified inputs, see text.

modified the deformation dependent parameters of the E1 strength function used in TALYS according to a new phenomenological parametrization. The improved new parametrization explains the experimental data better than the statistical models with default inputs and is discussed in the following section in detail.

### C. Phenomenological parametrization of the photon strength function

If one assumes that the dipole strength in a heavy nucleus is dominated by the GDR, then the strength function  $f_1(E_\gamma)$  according to Bartholomew et al. [40] is related to the average photoabsorption cross section  $\langle\sigma_\gamma(E_\gamma)\rangle$  by

$$\frac{\langle\sigma_\gamma(E_\gamma)\rangle}{3(\pi\hbar c)^2 \cdot E_\gamma} = f_1(E_\gamma) = \frac{\langle\Gamma_{E_1}\rangle}{E_\gamma^3 \cdot D}, \quad (6)$$

with  $\langle\Gamma_{E_1}\rangle$  and  $D$  denoting the average photon width and the average level spacing at the endpoint of electromagnetic transition. A new phenomenological description based on the ground state deformation parameters describes well the average photon absorption for nuclei with  $A > 80$  from  $E_x \approx 4$  MeV up to several MeV above the GDR [41].

A consistent description holds for the photon strength distribution in spherical, transitional, triaxial and well deformed nuclei. In nearly all nuclei the GDR is split

into two or three components, whose energies are well predicted by the finite range droplet model (FRDM) [42]. The splitting [43] is due to the three different axes of the ellipsoid parameterizing the nuclear shape with its deformation parameter  $\beta$  and triaxiality parameter  $\gamma$ :

$$E_k = \frac{E_0 \cdot R_0}{R_k} = \frac{E_0}{\exp \left[ \sqrt{\frac{5}{4\pi}} \cdot \beta \cdot \cos(\gamma - \frac{2}{3}k\pi) \right]} \quad (7)$$

This results from the fact that the vibrational frequency  $E_k/\hbar$  along a given axis  $k$  is inversely proportional to the corresponding semi-axis length  $R_k$ . The nuclear radius is given by  $R_0 = 1.16A^{1/3}\text{fm}$ . The GDR centroid energy  $E_0$  given in Ref. [42] of a spherical nucleus with mass  $A$  is calculated with an effective nucleon mass  $m^* = 874 \text{ MeV}/c^2$ .

The average absorption cross section in the GDR is given by

$$\langle \sigma_\gamma(E_\gamma) \rangle = \frac{1.29 \cdot Z \cdot N}{A} \sum_{k=1}^3 \frac{E_\gamma^2 \Gamma_k}{(E_k^2 - E_\gamma^2)^2 + E_\gamma^2 \Gamma_k^2} \quad (8)$$

where the GDR widths  $\Gamma_k$  to be used in the sum of up to three Lorentzians have been assumed to be constant, in contrast to earlier descriptions [44, 45]. The symbols  $E_\gamma$ ,  $E_k$  denote photon energy and resonance energies given in MeV and  $\langle \sigma_\gamma(E_\gamma) \rangle$  given in  $\text{fm}^2$ . The Thomas-Reiche-Kuhn sum rule as determined from general quantum mechanical arguments [46] is included in this description for the average photon absorption cross section obtained on an absolute scale.

The width  $\Gamma_k$  for the different components of the GDR is dependent on the resonance energy  $E_k$  and is generally used for all stable nuclei with  $A > 80$

$$\Gamma_k(E_k) = 1.99 \text{ MeV} \cdot \left( \frac{E_k}{10 \text{ MeV}} \right)^\delta, \quad (9)$$

where  $\delta = 1.6$  is taken from the one body dissipation model [43].

For the case of  $^{197}\text{Au}$  we assume that the average of the experimentally determined deformation parameters of the even-mass neighbor nuclei  $^{196}\text{Pt}$  and  $^{198}\text{Hg}$  [47, 48, 49] can be used to describe the shape of the odd nucleus  $^{197}\text{Au}$ , we insert  $\beta = 0.15$  and  $\gamma = 60^\circ$  into Eq. (7). The GDR centroid energy is  $E_0 = 13.9 \text{ MeV}$ . These parameters are in accordance with the FRDM and result in the following resonance energies and widths:  $E_{1,3} = 13.2 \text{ MeV}$ ,  $\Gamma_{1,3} = 3.1 \text{ MeV}$  and  $E_2 = 15.2 \text{ MeV}$ ,  $\Gamma_2 = 3.9 \text{ MeV}$ . The TALYS code was modified with these inputs for oblate deformation. The yield curve created using the cross sections resulting from modified inputs is shown in Fig. 9 and is in better agreement to the ELBE data.

The photon strength function of  $^{197}\text{Au}$  derived from different theoretical models and compared to experimental data is shown in Fig. 10. The strength function created using the modified inputs as discussed above is compared to the default models [44, 50] in TALYS which

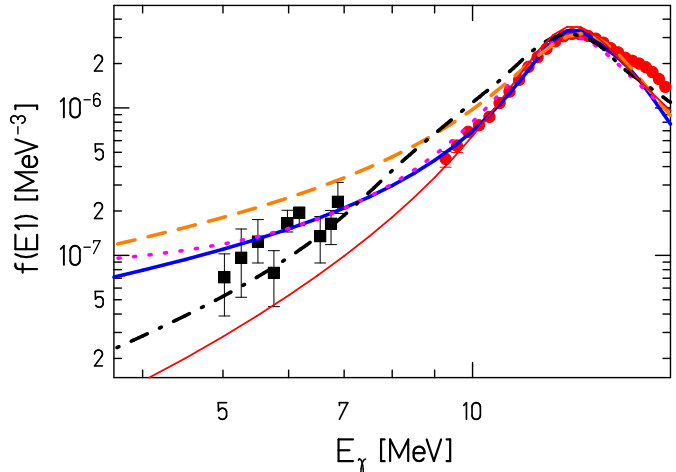


FIG. 10: (Color online) The photon strength function of  $^{197}\text{Au}$  derived on the assumption of oblate deformation (solid line) compared to different models. The dashed and dotted lines correspond to the strength functions given by Brink-Axel [50] and Kopecky-Uhl [44] models respectively. The microscopic E1 photoabsorption strength-functions determined within the QRPA model [51, 52] is shown by the dash-dotted line. All calculations were done using the TALYS Code. The Enhanced Generalized Lorentzian (EGLO) model taken from the Reference Input Parameter Library RIPL-2 of the IAEA [39] is shown as a thin solid line. The experimental strength function from Bartholomew et al. [40] (squares) below the neutron emission threshold and the strength function derived using the  $^{197}\text{Au}(\gamma, n)$  photoneutron cross section measured by Veyssiere et al. (circles) are also shown.

treats  $^{197}\text{Au}$  as a spherical nucleus. It is clear that the new parameters lead to a reduced strength at energies below the GDR and thus result in a good fit to its shape with a constant spreading width. This agrees well to the experimental strength function given by Bartholomew et al. [40] for energies below the neutron emission threshold. Above the separation energy, the strength functions shown were deduced from the  $^{197}\text{Au}(\gamma, n)$  cross sections by Veyssiere et al. The strength function derived using the modified parameters gives clearly a better fit to the data than calculations [51, 52] on the basis of the quasi particle random phase approximation (QRPA) with phenomenological correction for deformation.

## V. CONCLUSIONS

For the  $^{197}\text{Au}(\gamma, n)$  reaction, the activation yield has been measured and compared to the Hauser-Feshbach model calculations as well as previous experimental data. The measured activation yield at ELBE is in agreement to the calculated yields using cross sections measured with quasi-monoenergetic photons from positron annihilation in flight and laser-induced Compton backscattering.

The activation experiment discussed here, which was



performed in combination with a direct determination of the electron energy via the bremsstrahlung spectrum endpoint, deliver precise photon strength data. Thus they may allow a verification of data obtained previously by direct absorption experiments or by detecting neutrons from the  $(\gamma, n)$ -process. They also allow us to make judgements on parameterizations developed for the prediction of the photon strength function as well as on particle transmission functions, i.e. on optical model parameters.

We have demonstrated for the case of  $^{197}\text{Au}(\gamma, n)$  that a sum of two GDR-Lorentzians with a small oblate deformation of  $^{197}\text{Au}$  determining the energy split and the width difference describes the photon absorption well. The availability of information on the nuclear shape as well as on the PSF below threshold makes  $^{197}\text{Au}$  a prime case to perform a consistent test of statistical calculations of Hauser-Feshbach type and to derive a coherent picture of near-threshold processes. The detailed understanding of these has direct importance for the s-process as well, since the prediction of the relative abundances of the isotopes of Hg depends on the relative strength of

the  $\beta$ -decay of  $^{198}\text{Au}$  and  $^{198}\text{Au}(n, \gamma)$  in stellar plasmas. Last, but not least, the experimental data reported here for the  $^{197}\text{Au}(\gamma, n)$  reaction may serve as a normalization for future measurements on other nuclei. The  $^{197}\text{Au}(\gamma, n)$  reaction has been used as a photoactivation standard for the experiments discussed in Refs. [53, 54].

## VI. ACKNOWLEDGEMENTS

We thank Peter Michel and the ELBE team for providing a stable beam during activation experiments. We are indebted to E. Haug for providing valuable information about the theory of bremsstrahlung and his model codes. Special thanks to Rudi Apolle for simulating proton spectra of the deuteron breakup reaction under a realistic geometry. The technical assistance of Andreas Hartmann is gratefully acknowledged. We are grateful to Tom Cowan for a thorough, critical reading of the manuscript.

- 
- [1] W. Bothe and W. Gentner, *Zeitschrift für Physik* **106**, 236 (1937); **112**, 45 (1939).
  - [2] S. S. Dietrich and B. L. Berman, *Atomic Data and Nuclear Data Tables* **38**, 199 (1988).
  - [3] E. M. Burbidge, G. R. Burbidge, W. A. Fowler *et al.*, *Reviews of Modern Physics* **29**, 547 (1957).
  - [4] K. Sonnabend, P. Mohr, K. Vogt *et al.*, *Astrophysical Journal* **583**, 506 (2003).
  - [5] F. Käppeler and A. Mengoni, *Nuclear Physics* **A777**, 291 (2006).
  - [6] M. Arnould and S. Goriely, *Physics Reports* **384**, 1 (2003).
  - [7] K. Y. Hara, H. Harada, F. Kitatani *et al.*, *Journal of Nuclear Science and Technology* **44**, 938 (2007).
  - [8] P. Mohr, S. Brieger, G. Witucki *et al.*, *Nuclear Instruments and Methods A* **580**, 1201 (2007).
  - [9] G. Rusev, R. Schwengner, F. Dönaue *et al.*, *Physical Review C* **73**, 044308 (2006).
  - [10] G. Rusev, E. Grosse, M. Erhard *et al.*, *European Physical Journal A* **27** s01, 171 (2006).
  - [11] R. Schwengner, G. Rusev, N. Benouaret *et al.*, *Physical Review C* **76**, 034321 (2007).
  - [12] A. Wagner, R. Beyer, M. Erhard *et al.*, *Journal of Physics G-Nuclear and Particle Physics* **35**, 014035 (2008).
  - [13] G. Rusev, R. Schwengner, F. Dönaue *et al.*, *Physical Review C* **77**, 064321 (2008).
  - [14] R. Schwengner, R. Beyer, F. Dönaue *et al.*, *Nuclear Instruments and Methods A* **555**, 211 (2005).
  - [15] A. Wagner, R. Beyer, M. Erhard *et al.*, *Journal of Physics G-Nuclear and Particle Physics* **31**, S1969 (2005).
  - [16] H. Xiaolong, *Nuclear Data Sheets* **108**, 1093 (2007).
  - [17] GEANT3 : CERN program Library Long Writeup Q121, CERN, Geneva (CH), 1994.
  - [18] K. Debertin, R. G. Helmer, *Gamma- and X-ray spectroscopy with semiconductor detectors*, Elsevier Science Publ.(2001).
  - [19] G. Ruprecht, C. Vockenhuber, L. Buchmann *et al.*, *Physical Review C* **77**, 065502 (2008).
  - [20] F. Ajzenberg-Selove, *Nuclear Physics* **A506**, 1 (1990).
  - [21] S. J. Skorka, *Electromagnetic interaction in nuclear spectroscopy*, edited by W. D. Hamilton, North-Holland Publ., Amsterdam (1975).
  - [22] L. I. Schiff, *Physical Review* **83**, 252 (1951).
  - [23] S. M. Seltzer and M. J. Berger, *Atomic Data and Nuclear Data Tables* **35**, 345 (1986).
  - [24] E. Haug, *Radiation Physics and Chemistry* **77**, 207(2008).
  - [25] G. Roche, C. Ducos, and J. Proriol, *Physical Review A* **5**, 2403 (1972).
  - [26] F. Salvat, J. D. Martinez, R. Mayol *et al.*, *Physical Review A* **36**, 467 (1987).
  - [27] MCNP - Monte Carlo N-Particle Transport Code, <http://mcnp-green.lanl.gov/>; Version 4C2 obtainable from <http://www.nea.fr/abs/html/cc-0701.html>.
  - [28] M. Justus, U. Lehnert, P. Michel *et al.*, *Proceedings of DIPAC 2007 - 8th European Workshop on Beam Diagnostics and Instrumentation for Particle Accelerators*; 20.-23.05.2007; Venice, Italy. <http://www.elettra.trieste.it/dipac07/>, <http://www.jacow.org/>.
  - [29] B. L. Berman and S. C. Fultz, *Reviews of Modern Physics* **47**, 713 (1975).
  - [30] S. C. Fultz, J. T. Caldwell, R. L. Bramblett *et al.*, *Physical Review* **127**, 1273 (1962).
  - [31] B. L. Berman, R. E. Pywell, S. S. Dietrich *et al.*, *Physical Review C* **36**, 1286 (1987).
  - [32] A. Veyssiere, H. Beil, R. Bergere *et al.*, *Nuclear Physics* **A159**, 561 (1970).
  - [33] K. Vogt, P. Mohr, M. Babilon *et al.*, *Nuclear Physics* **A707**, 241 (2002).

- [34] G. M. Gurevich, L. E. Lazareva, V. M. Mazur *et al.*, Nuclear Physics **A338**, 97 (1980).
- [35] Y. I. Sorokin, V. A. Khrushchev, and B. A. Yurev, Izv. Akad. Nauk. SSSR, Ser. Fiz. **33**, 1891 (1973).
- [36] A. S. Penfold and J. E. Leiss, Physical Review **114**, 1332 (1959).
- [37] A. J. Koning, S. Hilaire and M. C. Duijvestijn, Proceedings of the International Conference on Nuclear Data for Science and Technology - ND2004, AIP vol. 769, eds. R.C. Haight, M.B. Chadwick, T. Kawano, and P. Talou, Sep. 26 - Oct. 1, 2004, Santa Fe, New Mexico, USA, p. 1154 (2005); <http://www.talys.eu>
- [38] T. Rauscher and F. K. Thielemann, Atomic Data and Nuclear Data Tables **88**, 1 (2004).
- [39] <http://www-nds.iaea.org/ripl-2/>, <http://www-nds.iaea.org.at/reports/indc-ccp-440.pdf>
- [40] G. A. Bartholomew, E. D. Earle, A. J. Ferguson *et al.*, Adv. Nucl. Phys. **7**, 229 (Plenum Press, New York, 1973).
- [41] A. R. Junghans, G. Rusev, R. Schwengner *et al.*, Physics Letters B, in press, doi:10.1016/j.physletb.2008.10.055.
- [42] W. D. Myers, W. J. Swiatecki, T. Kodama *et al.*, Physical Review C **15**, 2032 (1977); P.Möller, J.R. Nix, W.D. Myers *et al.*, Atomic Data Nuclear Data Tables **59** 185 (1995).
- [43] B. Bush and Y. Alhassid, Nuclear Physics **A531**, 27 (1991).
- [44] J. Kopecky and M. Uhl, Physical Review C **41**, 1941 (1990).
- [45] L. Zanini, F. Corvi, H. Postma *et al.*, Physical Review C **68**, 014320 (2003).
- [46] J. M. Eisenberg and W. Greiner, Nuclear Theory Vol. 2: *Excitation mechanisms of the nucleus* Third edition, North Holland Physics Publ., Amsterdam (1988).
- [47] A. Mauthofer, K. Stelzer, J. Idzko *et al.*, Zeitschrift für Physik A **336**, 263 (1990).
- [48] A. Bockisch, A. Bharuth-Ram, A. M. Kleinfeld *et al.*, Zeitschrift für Physik A **291**, 245 (1979).
- [49] N. J. Stone, Atomic Data and Nuclear Data Tables **90**, 75 (2005).
- [50] D. M. Brink, Nuclear Physics **4**, 215 (1957); P. Axel, Physical Review **126**, 671 (1962).
- [51] S. Goriely and E. Khan, Nuclear Physics **A706**, 217 (2002).
- [52] E. Khan, T. Suomijarvi, Y. Blumenfeld *et al.*, Nuclear Physics **A694**, 103 (2001).
- [53] C. Nair, A. R. Junghans, M. Erhard *et al.*, Journal of Physics G-Nuclear and Particle Physics **35**, 014036 (2008).
- [54] M. Erhard, A. R. Junghans, R. Beyer *et al.*, European Physical Journal A **27**, s01 135 (2006).